Substrate-dependent lateral order in naphthalene-tetracarboxylic-dianhydride monolayers

R. Fink, D. Gador, U. Stahl, Y. Zou, and E. Umbach
Experimentelle Physik II, Universität Würzburg, Am Hubland, D-97074 Würzburg, Germany
(Received 25 January 1999)

The lateral order of 1,4,5,8-naphthalene-tetracarboxylic-dianhydride (NTCDA) has been investigated on different metal substrates [Ag(100), Ag(111), Ag(110), Cu(100), and Ni(111)] mainly by low-energy electron diffraction. Film preparation under appropriate conditions leads to highly ordered (sub)monolayers of NTCDA on these covalently bonding substrates. On weakly interacting Ag(111) and Ag(100), two different superstructures are observed in each case which are related to each other by a reversible phase transition. In contrast, on Ag(110) and on the more reactive Cu(100) substrate only one superstructure exists. All superstructures are commensurate with the substrate because of chemisorption on specific adsorption sites. Adsorption of NTCDA on Ni(111) does not lead to a well-ordered monolayer due to a strong local bond and hence to a lower mobility. [S0163-1829(99)01528-3]

I. INTRODUCTION

Thin films of large organic π-conjugated molecules condensed on various substrates have attracted increasing attention during the past few years.[1–4] This is partly due to the potential applications of organic materials, especially for the design of improved, large-scale, and/or cheap optoelectronic devices[5,6] or sensors[7] and partly to the fact that rather little basic knowledge exists on such hybrid systems. Due to the variety of organic molecules and functional groups, the possibility of tailoring the electronic and optical properties of such films is a great advantage of organic materials.

Besides molecular properties, the morphology of the thin films and the interfaces also determine the properties of the possible devices. As for inorganic materials, crystalline imperfections influence the physical properties, e.g., the transport properties or the luminescence yield.[8] It is therefore important to prepare structurally well-ordered or, in the ideal case, epitaxial films. Organic molecular-beam deposition (OMBD) under ultrahigh-vacuum conditions has been demonstrated as a well-suited technique to prepare organic films of high structural quality.[1]

The molecule-substrate interface plays a major role in the growth of well-ordered organic films. Molecular disorder at the interface deteriorates the growth behavior of subsequent layers and no optimum (e.g., ideal layer-by-layer or step flow) growth is obtained. Although intermolecular van der Waals interaction and molecular shape, which often lead to appreciable polymorphism of organic crystals, allow a certain flexibility with respect to the molecular arrangement, the long-range order of the organic adsorbate is an important prerequisite for organic epitaxy. Molecular densities and arrangements at the interface, which are comparable to those in single crystals, favor the epitaxial growth of thicker layers.

In some cases, ideal substrate-molecule combinations were found, as, e.g., for perylene-tetracarboxylic-dianhydride (PTCDA) adsorbed on Ag(111).[1,9,10] There, the molecular arrangement in the monolayer fits well to that of the (102) plane in PTCDA,[11] and consequently well-oriented homogeneous films with a thickness of about 1000 layers were realized.[12] In contrast, x-ray-scattering investigations of PTCDA films on Au(111) reveal roughened films for equilibrium growth conditions.[13] For PTCDA/NTCDA (1,4,5,8-naphthalene-tetracarboxylic-dianhydride) heterostructures, quasiepitaxial growth was reported,[14] although their crystal structures are incommensurate.

The self-organization of organic monolayers is largely determined by the molecular mobility and the intermolecular interaction when inert substrates are employed. There is a variety of structural studies, in particular scanning-tunneling-microscopy (STM) investigations for large organic molecules on inert substrates such as highly oriented pyrolytic graphite (HOPG),[15–17] dichalcogenides (WSe_2, MoS_2),[4,18,19] SiO_2,[20] differently terminated GaAs substrates,[21] or InAs.[22] The weak interaction with the substrate often leads to the formation of incommensurate monolayers and polycrystalline films.

For more reactive substrates like metals, the molecule-substrate interaction is no longer negligible and may thus drastically influence the structural properties. Chemical bonds to the adsorbed molecules or to reactive subunits of the molecules may be formed, which hinder or influence the molecular self-arrangement in the film. Thus, to obtain structurally well-defined and perhaps tailored monolayers, it is necessary to achieve a proper relation between the molecule-substrate and the intermolecular interaction.

The formation of highly ordered films strongly prefers planar, highly symmetric molecules such as NTCDA (structural formula, see Fig. 1). The properties of interface interaction and film growth of this molecule on different substrates have thoroughly been investigated using different surface-sensitive techniques (STM, LEED, NEXAFS, TDS, XPS, UPS). The lateral order of the NTCDA monolayer on HOPG and MoS_2 has been investigated by LEED and STM with the result of two different monolayer structures as a function of coverage.[23] On these inert substrates the molecular plane is oriented parallel to the substrate in the low-coverage regime. In contrast, the molecules are oriented about perpendicular in densely packed monolayers reflecting the molecular arrangement of NTCDA single crystals.[24] STM and LEED investigations for NTCDA monolayers on the more strongly interacting Ag(111) substrate also reveal

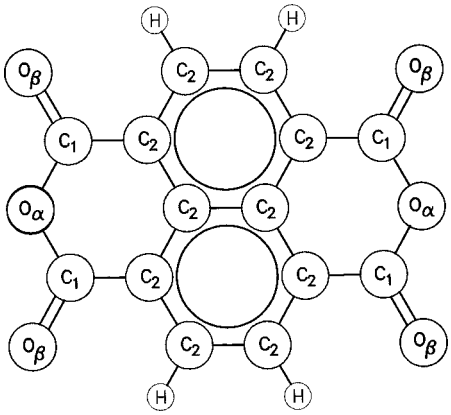

FIG. 1. Structural formula of 1,4,5,8-naphthalene-tetracarboxylic-dianhydride (NTCDA). Spectroscopically different C and O atoms are labeled differently.

two different structures.[25] However, in contrast to the inert substrates, the chemical interaction with the Ag(111) substrate (mainly through the naphthalene π system) forces the molecules into a molecular orientation with their molecular plane parallel to the substrate. The two monolayer structures can reversibly be transferred into each other by additional adsorption and desorption of small amounts (11% of a monolayer) of NTCDA molecules.[25]

In the multilayer regime, the molecular orientation depends mainly on the preparation conditions. In particular, substrate temperatures around 200 K lead to multilayers with planar orientation while temperatures above 280 K lead to molecules with perpendicular orientation.[26] The electronic interaction of the NTCDA molecules with different metals has also been investigated using different spectroscopic techniques [x-ray photoelectron spectroscopy (XPS), ultraviolet photoelectron spectroscopy (UPS), near-edge x-ray-absorption fine structure (NEXAFS)] (Refs. 27 and 28) reflecting the importance of the *d* density of states which significantly contributes to the molecule-substrate interaction. From previous NEXAFS experiments it is already known that the molecular plane of the NTCDA molecule in the monolayer is oriented parallel to the substrate for all metal substrates under investigation.[27]

The aim of the present paper is to demonstrate how the molecule-substrate interaction influences the lateral order in NTCDA monolayers, which in turn has consequences for the epitaxial growth of thicker organic films. For this purpose, the structural properties of NTCDA monolayers on various metals with different chemical reactivity and with different orientation are compared.[29,30]

II. EXPERIMENT

The experiments were performed in ultrahigh vacuum at a base pressure of about 2×10^{-10} mbar. The metal single-crystal substrates were prepared by repeated cycles of sputtering with Ar ions (kinetic energy: 700 eV) and subsequent annealing at 1000–1100 K depending on the substrate until no contamination was detected within the detection limits of XPS. High structural quality was achieved as controlled by low-energy electron diffraction (LEED). The NTCDA films were prepared by OMBD from a homemade Knudsen cell. The purity of the organic material, which has been outgased for several hours, and the deposition rate (calibrated by thermal desorption in conjunction with XPS, see, e.g., Chap. 3.1 of Ref. 25) were monitored by a quadrupole mass spectrometer (QMS). Evaporation rates were typically about 1 monolayer (ML) per minute. Substrate temperatures during deposition were chosen between 150 K and 250 K. To improve the quality of the LEED pattern, short annealing at 300–320 K was employed which resulted in the formation of large well-ordered domains. NTCDA films at coverages below $\theta<1$, i.e., in the submonolayer range ($\theta=1$ corresponds to saturation coverage), were prepared either by exact dosing (as controlled by the evaporation rate) or, for cases when NTCDA molecules could be desorbed, by (partial) thermal desorption from monolayer films (see below). Monolayers at saturation coverage ($\theta=1$) were prepared by thermal desorption of multilayers; the multilayer desorption peak was clearly separated from that of the monolayer in all cases. Note that the superstructures did not change upon annealing. The superstructures are given in the conventional matrix notation

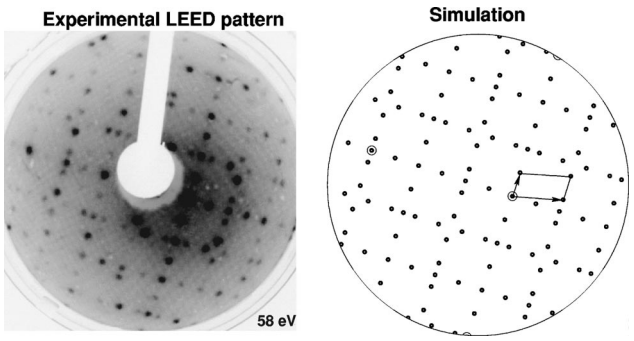

FIG. 2. Left: LEED pattern for NTCDA adsorbed on Ag(100) for a saturated monolayer ($\theta=1$) after deposition at 150 K and subsequent annealing at 320 K (electron energy: 58 eV); right: simulation of the LEED pattern according to the superstructure matrix $M_{C,100}$ reflecting the excellent agreement with the experimental data. Note that the specular reflex is slightly shifted from the center due to a small tilt of the sample with respect to the incoming electron beam. The reciprocal cell of one domain is also given.

$$\begin{pmatrix}\vec{b}_1\\ \vec{b}_2\end{pmatrix}=M\cdot\begin{pmatrix}\vec{a}_1\\ \vec{a}_2\end{pmatrix}\quad\text{and}\quad M=\begin{pmatrix}m_{11} & m_{12}\\ m_{21} & m_{22}\end{pmatrix},$$

which describes the base vectors $\vec{b}_1$ and $\vec{b}_2$ of the superstructure in terms of the unit vectors $\vec{a}_1$ and $\vec{a}_2$ of the substrate lattice. The superstructures are *commensurate* with the substrate, when all numbers m_{ij} $(i,j=1,2)$ of the matrix M are integer. Since in all cases the substrate spots could be observed simultaneously, the numbers of the derived crystallographic data are accurate to at least 5%.

III. RESULTS AND DISCUSSION

A. NTCDA monolayers on Ag(100)

Figure 2, left-hand side, shows a typical LEED pattern of a NTCDA monolayer on Ag(100) at saturation coverage ($\theta=1$) taken at 58 eV. The diffraction pattern reflects the fourfold symmetry of the substrate; it results from the incoherent superposition of four inequivalent domains. From simple tri-

TABLE I. Crystallographic data for NTCDA superstructures on various metal substrates as derived from LEED experiments. The data for Ag(111) have been derived from LEED and STM data and have already been published in Ref. 25.

NTCDA on	Ag(100)		Ag(111)		Ag(110)	Cu(100)
	relaxed	compressed	relaxed	compressed		
$M=$	$\begin{pmatrix} 3 & -3 \\ 4 & 4 \end{pmatrix}$	$\begin{pmatrix} 6 & -1.5 \\ 0 & 3 \end{pmatrix}$	$\begin{pmatrix} 4 & 0 \\ 3 & 6 \end{pmatrix}$	$\begin{pmatrix} 6 & -1 \\ 1 & 7 \end{pmatrix}$	$\begin{pmatrix} 3 & 0 \\ 1 & 3 \end{pmatrix}$	$\begin{pmatrix} 2 & -3 \\ 2 & 3 \end{pmatrix}$
Molecules/unit cell	2	2	2	4	1	1
$\lvert\vec{b}_1\rvert$	12.3 Å	17.8 Å	11.6 Å	19.0 Å	8.7 Å	9.2 Å
$\lvert\vec{b}_2\rvert$	16.4 Å	8.7 Å	15.0 Å	19.0 Å	12.6 Å	9.2 Å
$\angle(\vec{b}_1,\vec{b}_2)$	90°	104°	90°	120°	77°	112°
Area of unit cell	200.4 Å^2	150.4 Å^2	173.2 Å^2	311.2 Å^2	106.4 Å^2	76.2 Å^2
Area per molecule	100.2 Å^2	75.2 Å^2	86.8 Å^2	77.8 Å^2	106.4 Å^2	76.2 Å^2

angulation and identification of the first-order diffraction spots, the superstructure matrix

$$M_{C,100}=\begin{pmatrix} 6 & -1.5 \\ 0 & 3 \end{pmatrix}$$

can be easily deduced. The crystallographic data of this structure derived from the LEED pattern are shown in Table I. The unit cell consists of two NTCDA molecules, which is concluded from the size of the unit cell and the van der Waals size of the molecule. Due to the half-integer number in the above matrix, this superstructure can be regarded as commensurate to second order, since multiplication by 2 leads to a commensurate superstructure with integer numbers in the corresponding matrix and four molecules per unit cell. With the aid of the above superstructure matrix, it is possible to perform a geometric simulation of the LEED pattern using simple kinematic LEED theory taking into account only single scattering. The simulated LEED pattern including the superstructure unit cell in reciprocal space is shown on the right-hand side of Fig. 2. The comparison with the experimental data shows perfect agreement of the spot positions indicating that the derived matrix is correct.

After desorption of some NTCDA molecules upon thermal annealing (see below) or by film preparation with lower coverage ($\theta\approx 0.8$), another diffraction pattern is observed. The LEED pattern of this second structure taken for $\theta\approx 0.7$ at an electron kinetic energy of 63 eV is shown in Fig. 3. The analysis of the pattern of this superstructure yields the following superstructure matrix:

$$M_{R,100}=\begin{pmatrix} 3 & -3 \\ 4 & 4 \end{pmatrix}.$$

Again, two molecules contribute to the unit cell. The perfect agreement of the geometric simulation on the basis of this matrix (see the right-hand side of Fig. 3) and the experimental LEED pattern again corroborates the derived matrix. Comparing the crystallographic data of both superstructures given in Table I, one finds significant differences in the length of the two base vectors $\vec{b}_1$ and $\vec{b}_2$. More striking is the effect on the area of the unit cell which is 25% smaller for saturation coverage than for lower coverages. Due to the much higher density for $\theta\approx 1$, the corresponding superstructure is labeled *compressed monolayer*, whereas the superstructure in the low-coverage regime is denoted *relaxed monolayer*.

Unfortunately, LEED only yields periodicities and unit-cell data of the superstructures. The real-space configuration of the molecules within the unit cell cannot directly be derived from the LEED pattern. However, based on the crystallographic data summarized in Table I and the principle of minimal overlap of the atomic van der Waals radii of the molecules, it is possible to propose a real-space structure. In addition, the electrostatic field of the molecules, i.e., the quadrupole moment of the molecule due to the different partial charges on the anhydride oxygen atoms and the naphthalene core, can be taken into account. Thus plausible real-space arrangements of the molecules have been derived for both superstructures which are shown in Fig. 4.

In Fig. 4(b) the proposed real-space configuration for the relaxed monolayer is derived from the fact that there are two molecules in the unit cell, i.e., the long/short axis of the molecules should not coincide for nearest neighbors because of the electrostatic quadrupole field. The proposed structure is similar to what was found for the larger PTCDA molecule, which has a perylene instead of the naphthalene core. It was

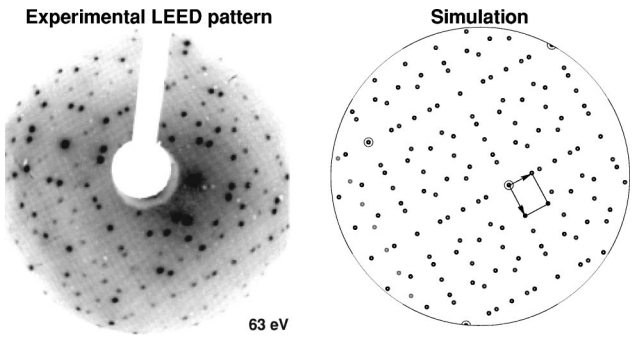

FIG. 3. Left: LEED pattern for NTCDA adsorbed on Ag(100) for a coverage of $\theta=0.7$ recorded after deposition at 150 K and subsequent annealing at 370 K (electron energy: 63 eV); right: simulation of the LEED pattern according to the superstructure matrix $M_{R,100}$. Note that the specular reflex is slightly shifted from the center due to a small tilt of the sample with respect to the incoming electron beam. The base vectors of the superstructure are included in the simulated LEED pattern. The reciprocal cell of one domain is also given.

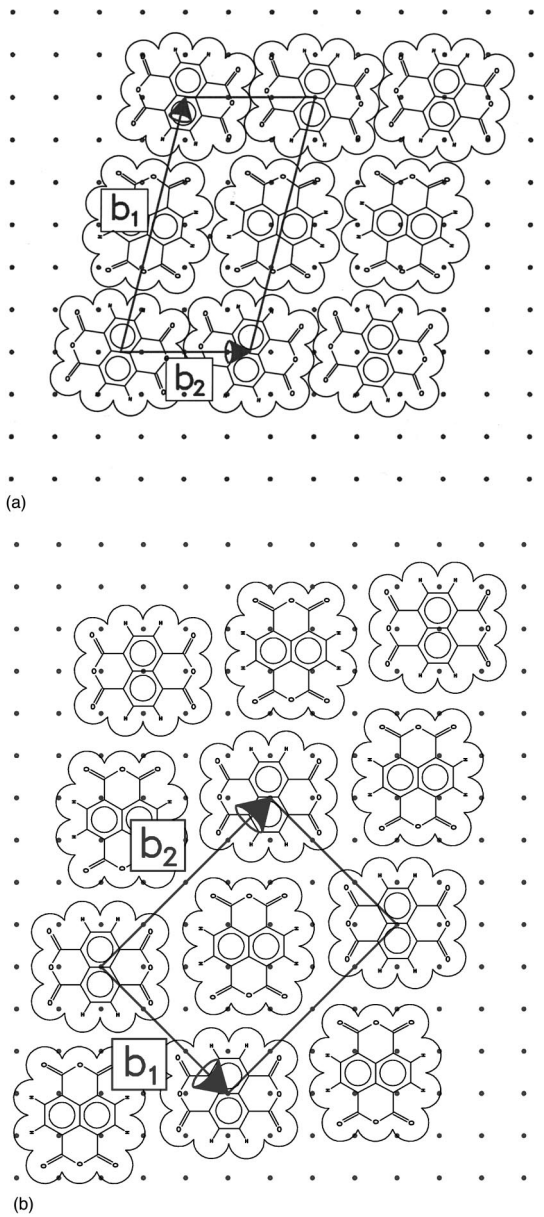

FIG. 4. Possible real-space configuration for the two NTCDA superstructures on Ag(100) derived from the crystallographic data on the basis of minimum overlap of the atomic van der Waals radii and of the experimental fact that two flat-lying molecules exist per unit cell. (a) Compressed monolayer and (b) relaxed monolayer.

argued that PTCDA has a significant quadrupole moment, which leads to the formation of a herringbone structure in layers of single crystals[11] or adsorbed layers on Ag(111).[1,9] Although the quadrupole moment of NTCDA should be smaller (because its aromatic core is smaller), the same argument should be applicable in the present case, too. Of course, a herringbone structure with a 90° angle between neighboring molecules is not compelling; in particular, the assumption that the molecules have equal distances to each other and do not form dimers has no direct justification. Thus, one could also consider a pairwise configuration of the molecules within a unit cell with smaller intermolecular distance.

The molecular configuration for the compressed monolayer shown in Fig. 4(a) is based on the arguments that two

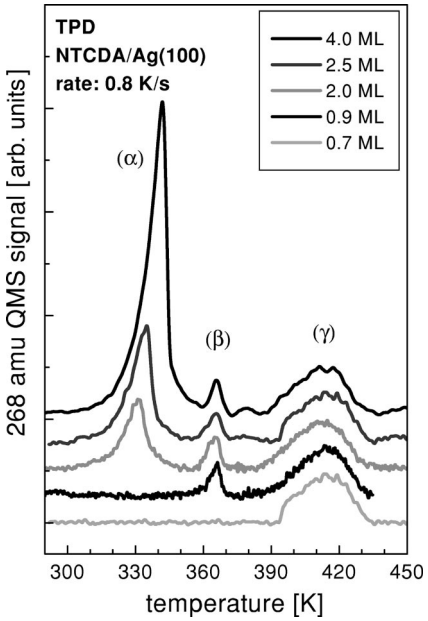

FIG. 5. Temperature-programmed desorption spectra for various NTCDA coverages on Ag(100) as indicated, recorded for a linear temperature ramp of 0.8 K/s using the QMS signal at 268 amu.

molecules per unit cell exist and that the overlap of the van der Waals radii of the molecules with their plane parallel to the substrate is minimum. The argument for minimum overlap is, of course, more rigorous in this case compared to the relaxed monolayer. The relative position of the two inequivalent NTCDA rows along the $\vec{b}_2$ direction is somewhat arbitrary but has been chosen to minimize the electrostatic intermolecular potential. Considering the experimental finding that the two superstructures can easily be transferred into each other, this transition requires the rotation and lateral movement of molecules based on the proposed real-space structures. In order to study this transition in more detail, temperature-programmed desorption (TPD) experiments have been performed, which shall be discussed next.

Figure 5 shows the TPD spectra for different coverages of NTCDA adsorbed on Ag(100) at 150 K. The QMS signal of NTCDA (molecular mass = 268 amu) was recorded while the sample temperature was increased linearly at a rate of 0.8 K/s. NTCDA multilayers show zero-order desorption kinetics with a desorption maximum at about 340 K for $\theta = 4$ ML [peak (α) in Fig. 4]. As expected for zero order, this maximum shifts to lower temperatures for lower coverages and is no longer observed for $\theta > 1$ ML. Multilayer desorption is already detected for $\theta = 2$ ML, i.e., the second layer is similarly bonded as higher layers in thicker films. This finding is in agreement with photoemission and NEXAFS data.[26–28] The electronic structure of the second layer was found to be identical to that of thicker films ($\theta = 50$ ML), i.e., the molecular interaction of the second layer is similar to that in NTCDA bulk material.[27]

For all coverages between 0.9 ML and 4 ML, a relatively sharp desorption peak at about 365 K [denoted by (β)] and a broad intensity distribution (γ) with its center around 410 K are detected (desorption signals at higher temperatures are due to desorption from the sample holder, as checked separately). Peak (γ) is also observed for lower coverages

(shown for $\theta = 0.7$ ML in Fig. 4). This broad distribution is attributed to desorption from the relaxed monolayer. The fact that this TPD peak does not look like one obtained for conventional zero- or first-order desorption kinetics can be explained by intermolecular interaction and/or a complicated desorption pathway, perhaps including some reorganization of the molecules on the surface. The desorption of large organic molecules from the monolayer on a metallic substrate is rarely observed. In the present case, it indicates a relatively weak bonding to the substrate as was already reported for NTCDA on Ag(111) (Ref. 25) or concluded from photoemission and x-ray absorption.[27]

With the assignment of peak (γ) to the *relaxed* monolayer, it is straightforward to attribute peak (β) to the desorption of the excess molecules during the phase transition from the compressed to the *relaxed* monolayer. The observation of unusually sharp TPD peaks in the case of a structural phase transition has been made earlier; it has been attributed to a kind of ''autocatalytic'' effect induced by the rearrangement and adsorption site optimization of the remaining molecules upon desorption of the excess molecules which lead to the compression. The identification of peak (β) is furthermore corroborated by the finding that the integral intensity of (β) is (within experimental uncertainty) identical for all coverages higher than $\theta = 1$ ML and accordingly smaller for $\theta = 0.9$ ML. The peak intensity ratio of (β) to (γ) of 23% fits approximately to the ratio derived from the geometrical data of the two superstructures, e.g., from the comparison of the areas per molecule of the respective structures (see Table I). A leading-edge quantitative analysis of the two peaks (α) and (β) yields a desorption energy of 68 ± 10 kJ/mol and 95 ± 10 kJ/mol for multilayer desorption and for the reconfiguration of the monolayer, respectively.

Finally, the phase transition between the relaxed and compressed phase is found to be reversible as tested by repeated cycles of adsorption and subsequent desorption of small amounts of NTCDA. The LEED pattern changed accordingly from the relaxed to the compressed phase and vice versa. It is worth noting that the difference in the desorption maxima of (β) and (γ) is much larger here than for Ag(111), where a similar phase transition was found.[25] This indicates different molecular reorganization mechanisms and bonding strengths for both adsorbate systems. For instance, the difference could be due to comparable bonding strengths for the various adsorption sites of both phases on Ag(111) (leading to similar desorption energies) and to different bonding strengths for those on Ag(100). An alternative or additional reason could be that the compression of the molecules and hence the repulsive interaction is even stronger on Ag(100) compared to Ag(111) leading to a reduction of the activation energy for peak (b) in the present case. The actual geometry parameters are in support of this argument (see Table I). At present this explanation, however, remains speculative. To get deeper insight into the dynamics of the phase transition, real-time experiments monitoring the domain growth of the relaxed phase and the rearrangement during the phase transition are highly desirable, which could be performed during thermal desorption of NTCDA. Scanning tunneling microscopy (STM) or high-resolution low-energy electron microscopy (LEEM) (Ref. 29) would be a proper choice of methods for this experiment.

B. NTCDA monolayers on Ag(111)

LEED and STM results on the lateral order of NTCDA monolayers adsorbed on Ag(111) were presented recently in detail in Ref. 25, and shall only be summarized here for completeness. As for the Ag(100) substrate, two different superstructures were observed. For coverages close to $\theta = 1$ a densely packed monolayer ($\rightarrow$ *compressed monolayer*) described by

$$M_{C,111} = \begin{pmatrix} 6 & -1 \\ 3 & 6 \end{pmatrix}$$

has been found with four NTCDA molecules per unit cell. At lower coverages ($\theta \leqslant 0.85$ ML) another commensurate superstructure ($\rightarrow$ *relaxed monolayer*) with

$$M_{R,111} = \begin{pmatrix} 4 & 0 \\ 3 & 6 \end{pmatrix}$$

and two molecules per unit cell has been observed. The density of the latter structure is only 90% of the density of the compressed monolayer in agreement with the quantitative result of thermal desorption spectroscopy. As for Ag(100), these two superstructures can be reversibly transferred into each other by adsorption/desorption of NTCDA molecules, i.e., they are related to each other by a reversible structural phase transition. As mentioned above, the desorption peak from the compressed monolayer (β) is in this case much closer to the desorption peak from the relaxed monolayer (γ), i.e., the difference in activation energy is much smaller than for Ag(100). At intermediate NTCDA coverages, both structures coexist. Due to the good compatibility of both superstructures (i.e., they have one common vector of their unit cells and hence are commensurate to each other in this direction), a striplike arrangement of domains of the two different structures is formed as confirmed by STM. Thus, sharp and straight phase boundaries limit the single domains.[25] Since to date no STM data are available for NTCDA/Ag(100), direct comparison of the domain boundaries is impossible. The geometric data for NTCDA/Ag(111) are summarized in Table I.

C. NTCDA monolayers on Ag(110)

Also in the case of NTCDA on the lower-symmetry surface Ag(110), high-quality LEED patterns were obtained. However, in contrast to the above-mentioned results from Ag(100) and Ag(111), only one superstructure was observed. A LEED pattern taken from a saturated NTCDA monolayer ($q = 1$) at a kinetic energy of 54 eV is shown in Fig. 6(a). According to the twofold symmetry of the substrate, the LEED pattern is twofold symmetric. The analysis of the LEED pattern leads to the superstructure matrix

$$M_{110} = \begin{pmatrix} 3 & 0 \\ 1 & 3 \end{pmatrix}.$$

Based on this matrix, the simulation of the LEED pattern was performed [shown in Fig. 6(b)]. The comparison with the experimental data again shows a perfect agreement, which indicates that the superstructure matrix describes the experimental data correctly. The analysis of the obtained

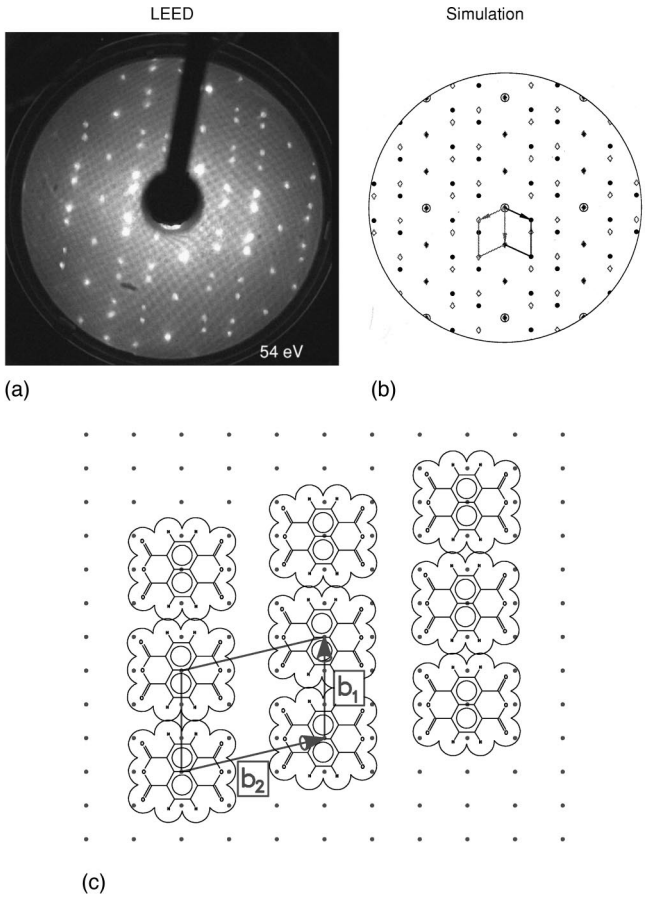

FIG. 6. (a) LEED pattern for NTCDA adsorbed on Ag(110) for saturation coverage (electron energy: 54 eV). (b) Simulation of the LEED pattern according to the superstructure matrix M_{110}. The base vectors of the superstructure are included in the simulated LEED pattern. (c) Suggested real-space structure for the lateral arrangement of the NTCDA molecules.

crystallographic data shown in Table I indicates that the unit cell contains only one NTCDA molecule. This is also in contrast to the monolayer structures on Ag(111) and Ag(100). In addition, the geometric structure on Ag(110) is very open compared to those on the other surface orientations. The real-space structure based on the derived superstructure yields a rowlike structure parallel to the Ag rows. The molecular arrangement within the rows as well as the position of these rows with respect to the densely packed rows of the substrate atoms, of course, cannot be deduced from the LEED data. The proposed structure in Fig. 6(c) is based on two arguments: one is that adsorption sites usually are highly symmetric with respect to the substrate, at least in the case of strong chemisorption and relatively low adsorbate density. The other is based on the comparison with PTCDA/Ag(110) for which a very similar adsorption site has unambiguously been determined using STM (Ref. 9) (see also Ref. 30). In the present case, the anhydride oxygens may lock into identical positions, since the O-O distances (for isolated molecules) are very close to the Ag-atom distances along the $[1\bar{1}0]$-substrate axis. Of course, a slight shift of the molecular rows parallel and/or perpendicular to the [110] direction by half a substrate surface lattice constant as well as a slight rotation to further minimize the overlap of the atomic van der Waals radii of the NTCDA molecules cannot be completely excluded. The answer to this question would require a detailed STM investigation such as that of Ref. 31.

As mentioned, a similar molecular arrangement was also found for PTCDA adsorbed on Ag(110). In that case, a brick-wall-type arrangement of molecules with the short molecular axis parallel to the Ag$[1\bar{1}0]$ rows was concluded from STM investigations.[9] From the simultaneous observation of PTCDA molecules and Ag substrate atoms, the position of PTCDA with respect to the substrate was exactly determined.[32] The center of the PTCDA molecule is located between two close-packed Ag rows. Comparing the size of the NTCDA molecule with that of PTCDA along the long molecular axis, the difference is about the distance of neighboring densely packed Ag rows. Therefore, one may conclude that the anhydride groups are similarly bound to the Ag(110) substrate in both cases. The experimental verification of this interpretation would of course be very interesting.

D. NTCDA monolayers on Cu(100)

On Cu(100) the NTCDA monolayer is also very well ordered as indicated by the sharp LEED spots and low background intensity [Fig. 7(a)]. As for Ag(100) the LEED pattern has fourfold symmetry. However, in contrast to the Ag(100) substrate only one superstructure for the NTCDA monolayer could be prepared for coverages ranging from $\theta = 0.5$ to $\theta = 1$. The superstructure matrix

$$M = \begin{pmatrix} 2 & -3 \\ 2 & 3 \end{pmatrix}$$

was derived from the experimental LEED pattern. Again, a commensurate superstructure is formed, i.e., the NTCDA molecules adsorb on identical adsorption sites within a domain. The perfect agreement between the simulation [Fig. 7(b)] and the experimental data indicates the correctness of this matrix. The analysis of the LEED pattern delivers the crystallographic data shown in Table I. From the size of the unit cell and the NEXAFS result of oriented molecules parallel to the substrate,[28] it can be concluded that the unit cell contains only one molecule. This is in contrast to both monolayer structures on Ag(100), which contain two NTCDAmolecules per unit cell. The interesting finding is that the molecules are as densely packed as for the compressed monolayer on Ag(111) and nearly as densely as that on Ag(100).

The fact that there is only one molecule per unit cell leads to the conclusion that all molecules are aligned parallel to each other. Therefore, it is almost straightforward to propose a real-space structure for this adsorbate system. Based on the criterion of minimum overlap of the van der Waals radii, the model in Fig. 7(c) is favored. The occurrence of a quadrupole moment, which, however, may be markedly reduced by the adsorption bond, probably leads to the displacement of the molecules for neighboring rows along the $\vec{b}_1 + \vec{b}_2$ direction, which minimizes the electrostatic energy under the given circumstances.

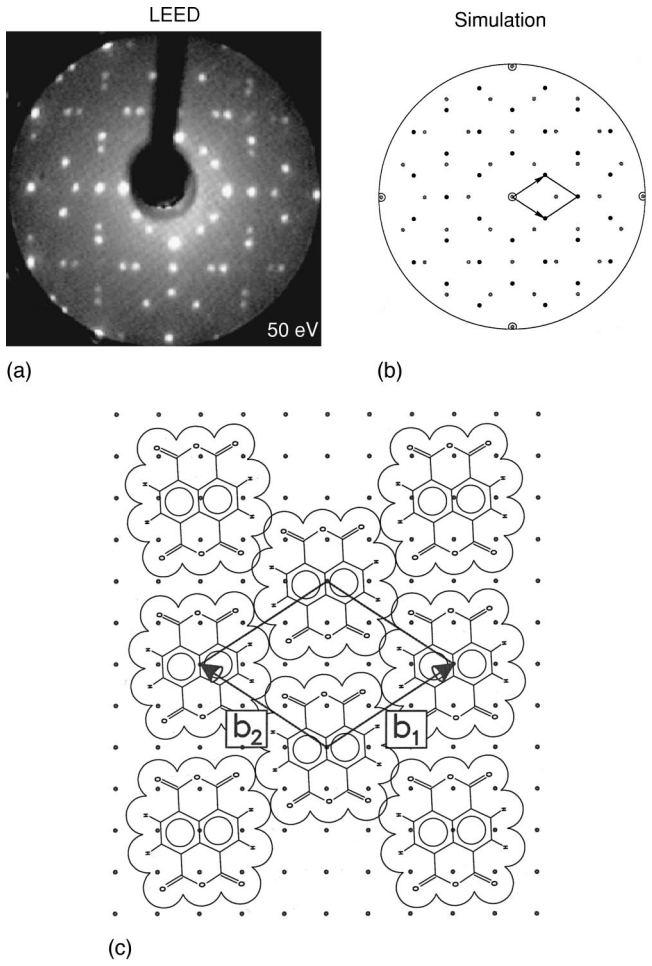

FIG. 7. (a) LEED pattern for NTCDA adsorbed on Cu(100) for a saturated monolayer (electron energy: 50 eV). (b) Simulation of the LEED pattern according to the superstructure matrix $M_{\mathrm{Cu},100}$. The base vectors of the superstructure are included in the simulated LEED pattern. (c) Suggested real-space structure for the lateral arrangement of the NTCDA molecules.

E. NTCDA monolayers on Ni(111)

Several tests to prepare well-ordered NTCDA monolayers on Ni(111) failed, although the parameters for the preparation conditions were varied over a wide range. In particular, substrate temperatures close to the desorption temperature for NTCDA monolayers from Ag were utilized. Nevertheless, no reasonable LEED patterns were observed, i.e., no long-range-ordered domains were formed on this substrate. Long-range-ordered domains are only formed if the molecules remain intact and are sufficiently mobile, thus enabling self-organization in the molecular adsorbate layer. Since the internal (vibrational and rotational) energy of adsorbing molecules is, of course, identical for the various substrates, the energy accommodation must be different for Ni(111) as compared to the other substrates, i.e., the kinetic, rotational, and vibrational energy of the impinging molecule is rapidly transferred into the substrate. Thus, in the case of Ni(111) the molecules hit and stick while for the other substrates they remain sufficiently mobile to form large ordered domains.

In the case of Ni(111) it is very likely that a strong local chemical bond is formed between the substrate and the reactive subunits of NTCDA (in particular, the anhydride oxygen atoms). This is corroborated by the NEXAFS data, which clearly demonstrate the stronger influence of the Ni substrate on both the interaction with the naphthalene core and that with the anhydride. The strong π interaction forces the molecular planes to be oriented parallel to the substrate, as also found for the other metal substrates.[27]

From these findings, Ni(111) cannot be regarded as an ideal substrate for the epitaxy of anhydride molecules. Astonishingly, the smaller anhydride NDCA (naphthalene ring with only one dianhydride group) forms an ordered superstructure on Ni(111) at coverages below 0.7.[33,34] In that case, the interaction of just one anhydride with the substrate is apparently smaller. Thus the lateral mobility of the NDCA molecules can be larger and self-organization to form long-range-ordered domains is possible. However, for PTCDA on Ni(111) also no long-range order has been found.[35] Although NEXAFS data clearly prove flat-lying molecules which are intact according to XPS, UPS, and NEXAFS (Ref. 12) ordering also does not occur as could be monitored by STM,[1] similar to the present case. We believe that a similar hit-and-stick mechanism due to a strong local bond is responsible for the lack of order. In other words, the lateral corrugation of the bonding potential seems to be too high in both cases, such that diffusion is impossible up to the temperature (about 650 K) at which the molecules start to decompose.[27,36]

IV. CONCLUDING REMARKS

In contrast to inert surfaces like HOPG and MoS_2, the NTCDA monolayers on most of the investigated low-index metal substrates are commensurate with the substrate. The commensurability can be determined with high reliability, since first the zero-order spots of the unreconstructed substrate can be monitored simultaneously, and second in some cases the commensurate superstructures have coincident LEED spots from different symmetry-equivalent domains. Thus, the finding of commensurate monolayer films is more reliably derived from LEED rather than from STM data, which require a very accurate calibration or a simultaneous observation of the substrate atoms.

The formation of commensurate superstructures on metal substrates is not just accidental. Comparing the various superstructures, one finds very different molecular densities in the monolayers. One can therefore conclude that the (lateral) intermolecular interactions are less important and that the commensurability of the superstructure is mainly caused by the strong vertical interaction of the adsorbed molecules with the various substrates.

A different degree of substrate interaction is observed in the thermal desorption spectra (see above and Ref. 25), which show monolayer desorption for all Ag surfaces but no signal of intact molecules from the monolayers on Cu(100) and Ni(111), i.e., in these cases the molecules dissociate before they desorb as monitored by XPS and NEXAFS. In addition, the chemical interaction with the various metal substrates is evident from the NEXAFS spectra taken at the C and O K edges of NTCDA monolayers.[27] The strong modifications of the π^* resonances, in particular for the O spectra, clearly indicate the chemisorptive bonding of the NTCDA molecules to these metals. For the Ag substrates,

the chemisorptive bond occurs predominantly via the π system (especially through the LUMO and LUMO+1). It is relatively weak as concluded from the relatively small modification of the NEXAFS resonances when reducing the film thickness from NTCDA multilayers to the monolayer. The chemisorptive bonding to the substrate is much stronger for Cu(100) and especially for Ni(111) as derived from the NEXAFS data.[27] For Ni(111) substrates, even fragmentation of the NTCDA molecules has to be taken into consideration, at least for temperatures above room temperature. For annealed NTCDA monolayers on Ni(111), fragmentation is most probable.

The NEXAFS results and the fact that for NTCDA on Ni(111) no LEED pattern has been obtained, indicate that the interaction of the NTCDA molecules with this substrate is so strong and local that the molecules are not mobile enough to form a long-range order, whereas the mobility on Ag and Cu substrates is still high enough. On Ag(111) and Ag(100) the lateral corrugation of the bonding potential is probably small enough to enable both relaxed and compressed monolayer structures, whereas the stronger interaction between copper, or even Ag(110), and NTCDA hinders this polymorphism.

From the LEED results it is evident that the substrate orientation plays the dominant role in the formation of the monolayer superstructures. The real-space structures are very different for the six cases discussed in this paper. Moreover, only one monolayer structure has been observed for NTCDA on Ag(110), whereas on Ag(111) and Ag(100) two different monolayer structures have been found. Because the ''*global*'' electronic properties of the various Ag surfaces are very similar, the specific local bonding must be the main reason for this different behavior. Due to the row-valley structure of the Ag(110) substrate, which leads to a stronger lateral corrugation of the bonding potential, the formation of a more densely packed (compressed) monolayer is prevented and therefore only one relatively open monolayer structure is obtained.

A strong substrate interaction is also advantageous for the LEED investigation itself. The LEED patterns on Cu(100) are very stable against electron bombardment. No damaging effects were observed upon electron bombardment up to 500 eV kinetic energy or x-ray illumination with Mg $K\alpha$ radiation ($h\nu = 1253.6$ eV) over several hours. In contrast, the quality of the LEED pattern on Ag substrates got worse on a time scale of less than 2 h, which is explained by the fact that electron-induced excitations cannot relax into the substrate as efficiently as for the more strongly bound molecules. Thus, fragmentation of molecules occurs on Ag(111) with slightly increased probability as compared to Cu(100), which then in turn negatively influences the lateral order.

From the above results it can be seen that the formation of well-ordered NTCDA monolayers on different substrates strongly depends on several parameters. If the substrate interaction is very weak (e.g., for HOPG, MoS_2) the lateral molecular arrangement is governed by the intermolecular interactions. In contrast, the stronger interaction with metals leads to the formation of substrate-induced (commensurate) superstructures. It should be noted, however, that only metal substrates with strongly bound *d* electron (i.e., noble metals) appear to be suitable because of their weaker chemical interaction with adsorbates, while metals with *d* states at the Fermi level are apparently too reactive for lateral ordering, probably because the potential at the optimum adsorption site is too deep to allow diffusion.

Reduced molecular mobility as observed for NTCDA and PTCDA on Ni(111) or PTCDA on Si(111) and Ge(100) also turned out to have negative consequences for epitaxial growth.[1,37] We predict that this is true for all *d* metals with partly filled *d* shells, and that in some cases (partial) dissociation may occur, even at room temperature or below. Finally, the knowledge of the structural order at the organic-substrate interface is important for the evaluation of OMBE processes independent of the advantage that large organic molecules may crystallize in different crystalline modifications (polymorphism). Stress within the organic film leads to metastability as, e.g., observed for NTCDA multilayer films. Only for NTCDA on Cu(100) did we observe the same high lateral order as is in the monolayer even for 5 ML, which, at first glance, is surprising as no such layers are formed in NTCDA single crystals. This must mean that metastable crystalline films can be formed by nonequilibrium growth on a properly ordered interface. This very interesting finding requires further investigations, which are underway. We note that up to now ideal epitaxial growth (with identical lateral order in all layers) has only been found for PTCDA on Ag(111),[1,12,38] for which even 1000-Å-thick films with high structural order could be grown.

ACKNOWLEDGMENTS

We are very grateful to Professor Dr. N. Karl (Universität Stuttgart) for the ultrapure NTCDA material, to Dr. M. Sokolowski for fruitful discussions, and to U. Herber for assistance in preparing the figures. This work has been financially supported by the BMBF (Projects No. 05 625 WWA 9 and 05 SF8 WWA 7). One of us (E.U.) thanks the Fond der Chemischen Industrie for support.

[1] E. Umbach, M. Sokolowski, and R. Fink, Appl. Phys. A: Mater. Sci. Process. **63**, 565 (1996).

[2] B. G. Frederick, Q. Chen, S. M. Barlow, N. G. Condon, F. M. Leibsle, and N. V. Richardson, Surf. Sci. **352**, 238 (1996).

[3] T. J. Schuerlein and N. R. Armstrong, J. Vac. Sci. Technol. A **12**, 1992 (1994).

[4] M. Möbus, N. Karl, and T. Kobayashi, J. Cryst. Growth **116**, 65 (1992).

[5] H. Neureiter, W. Gebauer, C. Väterlein, M. Sokolowski, P. Bäuerle, and E. Umbach, Synth. Met. **67**, 173 (1994).

[6] M. Meier, M. Cölle, S. Karg, E. Buchwald, J. Gmeiner, W. Riess, and M. Schwoerer, Mol. Cryst. Liq. Cryst. Sci. Technol., Sect. A **283**, 197 (1996).

[7] T. Katsume, M. Hiramoto, and M. Yokoyama, Appl. Phys. Lett. **69**, 3722 (1996).

[8] W. Gebauer, M. Bässler, R. Fink, M. Sokolowski, and E. Umbach, Chem. Phys. Lett. **266**, 177 (1997).

[9] K. Glöckler, C. Seidel, A. Soukopp, M. Sokolowski, E. Umbach,

M. Böhringer, R. Berndt, and W. Schneider, Surf. Sci. **405**, 1 (1998).
[10] C. Seidel, Ph.D. thesis, Universität Stuttgart, (1993).
[11] M. Möbus, N. Karl, and T. Kobayashi, J. Cryst. Growth **116**, 495 (1992).
[12] J. Taborski, P. Väterlein, H. Dietz, U. Zimmermann, and E. Umbach, J. Electron Spectrosc. Relat. Phenom. **75**, 129 (1995).
[13] P. Fenter, F. Schreiber, L. Zhou, P. Eisenberger, and S. R. Forrest, Phys. Rev. B **56**, 3046 (1997).
[14] F. F. So, S. R. Forrest, Y. Q. Shi, and W. H. Steier, Appl. Phys. Lett. **56**, 674 (1990).
[15] R. Heinz, A. Stabel, J. P. Rabe, G. Wegner, F. C. De Schryver, D. Corens, W. Dehaen, and C. Süling, Angew. Chem. **20**, 106 (1994).
[16] J. E. Freund, M. Edelwirth, P. Kröbel, and W. M. Heckl, Phys. Rev. B **55**, 5394 (1997).
[17] P. E. Burrows, Y. Zhang, E. I. Haskal, and S. R. Forrest, Appl. Phys. Lett. **61**, 2417 (1992).
[18] C. Ludwig, B. Gompf, J. Petersen, R. Strohmaier, and W. Eisenmenger, Z. Phys. B **93**, 365 (1994).
[19] D. P. E. Smith, W. M. Heckl, and H. Klagges, Surf. Sci. **278**, 166 (1992).
[20] O. Böhme, Ch. Ziegler, and W. Göpel, Adv. Mater. **6**, 587 (1994).
[21] Y. Hirose, S. R. Forrest, and A. Kahn, Phys. Rev. B **52**, 14 040 (1995); Appl. Phys. Lett. **66**, 944 (1995).
[22] C. Kendrick and A. Kahn, Appl. Surf. Sci. **123/124**, 405 (1998).
[23] R. Strohmeier, C. Ludwig, J. Petersen, B. Gompf, and W. Eisenmenger, Surf. Sci. **351**, 292 (1996).
[24] L. Born and G. Heywang, Z. Kristallogr. **190**, 153 (1990).
[25] U. Stahl, D. Gador, A. Soukopp, R. Fink, and E. Umbach, Surf. Sci. **414**, 423 (1998).
[26] D. Gador, C. Buchberger, R. Fink, and E. Umbach, Europhys. Lett. **41**, 213 (1998).
[27] D. Gador, Y. Zou, C. Buchberger, M. Bertram, R. Fink, and E. Umbach, J. Electron Spectrosc. Relat. Phenom. (to be published).
[28] D. Gador, C. Buchberger, R. Fink, and E. Umbach, J. Electron Spectrosc. Relat. Phenom. **96**, 11 (1998).
[29] E. Bauer, Ultramicroscopy **36**, 62 (1991).
[30] C. Seidel, C. Awater, X. D. Liu, R. Ellerbrake, and H. Fuchs, Surf. Sci. **371**, 123 (1997).
[31] M. Böhringer, W. D. Schneider, R. Berndt, K. Glöckler, M. Sokolowski, and E. Umbach, Phys. Rev. B **57**, 4081 (1998).
[32] M. Böhringer, W.-D. Schneider, K. Glöckler, E. Umbach, and R. Berndt, Surf. Sci. **419**, L95 (1998).
[33] R. Li, Ph.D. thesis, Universität Stuttgart (1994).
[34] E. Umbach, C. Seidel, J. Taborski, R. Li, and A. Soukopp, Phys. Status Solidi B **192**, 389 (1995).
[35] K. Glöckler, Ph.D. thesis, Universität Würzburg (1997).
[36] M. Jung, U. Baston, T. Porwol, H.-J. Freund, and E. Umbach, (unpublished).
[37] E. Umbach, K. Glöckler, and M. Sokolowski, Surf. Sci. **402–404**, 20 (1998).
[38] L. Kilian, M. Sokolowski, and E. Umbach (unpublished).